www.dergipark.gov.tr
ISSN:2148-3736
El-Cezerî Fen ve Mühendislik Dergisi
Cilt: 7, No: 1, 2020 (189-197)

El-Cezerî Journal of Science and Engineering
Vol: 7, No: 1, 2020 (189-197)
DOI: 10.31202/ecjse.612105

ECJSE

Research Paper / Makale

Constant Current/Voltage Charging of A 250W E-Bike with Wireless Power Transfer

Murat BAYRAKTAR*, Emin YILDIRIZ

Düzce Üniversitesi, Mühendislik Fakültesi,Elektrik-Elektronik Mühendisliği Bölümü, 81620 Düzce/TÜRKİYE
bayraktarmrt001@gmail.com

Received/Geliş: 27.08.2019 **Accepted/Kabul:** 28.10.2019

Abstract: Practical and safely charge of the electric vehicle become important as their use increases. In Turkey, the use of electric bicycles (less than 250 W), which do not require special driving licenses, has increased remarkably in recent years. In this study, a system for wireless charging has been developed to practice the charging of e-bikes. The charging of the 36V battery bank on the e-bike is achieved with 72% overall system (DC/DC) efficiency. The air gap is 75 mm due to the wheel diameter and the bicycle chassis. The switching frequency on the transmitter side is selected as 20 kHz for inductive power transfer. On the secondary side, a charge regulator is designed to charge the battery according to its characteristic. The constant current and constant voltage modes can be performed according to battery characteristic. Besides being practical and reliable, the overall performance of the developed system can compete with the conventional cable charging system.

Keywords: E-bike; wireless power transfer, battery charging.

250W Elektrikli Bisikletin Kablosuz Güç Aktarımı ile Sabit akım/Gerilim Modunda Şarjı

Öz: Elektrikli araçların kullanımı arttıkça; bu araçların pratik ve güvenli şekilde şarj edilmesi, önemli bir araştırma konusu olmuştur. Türkiye'de özel ehliyet gerektirmeyen elektrikli bisiklet kullanımı (250 W'tan daha az), son yıllarda önemli ölçüde artmıştır. Bu çalışmada elektrikli bisikletler için kablosuz şarj sistemi geliştirilmiştir. E-bisiklet üzerindeki 36V'luk batarya bankı, %72 genel sistem verimiyle (DC-DC) kablosuz olarak şarj edilmiştir. Temassız güç aktarım hava aralığı, tekerlek çapı ve bisiklet şasesi dikkate alınarak 7.5 cm olarak belirlenmiştir. Primer tarafındaki anahtarlama frekansı, endüktif güç aktarımını sağlamak için 20 kHz olarak seçilmiştir. Sekonder tarafta ise batarya karakteristiğine uygun olarak çalışan bir şarj regülatörü geliştirilmiştir. Bu regülatör ile batarya karakteristiğine uygun olarak, sabit akım ve sabit gerilim kipinde şarj yapılabilmektedir. Böylece geliştirilen kablosuz şarj sistemi; pratik ve güvenilir olmasının yanı sıra, performans olarak da geleneksel kablolu şarj sistemi ile rekabet edebilir seviyededir.

Anahtar kelimeler: Elektrikli bisiklet; kablosuz güç aktarımı, batarya şarjı

1. Introduction

There is a growing interest in electric vehicle technology (EV) all over the world. With the widespread use of EVs, safe and fast charging attracts researchers. Wireless power transfer (WPT) removes cable clutter to provide safer operation. Further, it is not affected by weather conditions and user errors. WPT for EVs has been done at different air-gap in the literature. Table 1 lists some applications. WPT can be basically divided into two categories microwave power transfer (MPT) and inductive power transfer (IPT) according to the transmission frequency. In MPT, which operates in radio frequency, the primary coil is a transmitter antenna and the secondary coil works

How to cite this article
Bayraktar, M, Yıldırız, E., "*Constant Current/Voltage Charging of A 250W E-Bike with Wireless Power Transfer*" El-Cezerî Journal of Science and Engineering, 2020, 7 (1); 189-197.

Bu makaleye atıf yapmak için
Bayraktar, M, Yıldırız, E., *"250W Elektrikli Bisikletin Kablosuz Güç Aktarımı ile Sabit akım/Gerilim Modunda Şarjı"* El-Cezerî Fen ve Mühendislik Dergisi 2020 7 (1); 189-197.

like a receiver antenna. MPT, which operates at frequencies in MHz, is commonly used in biomedical devices, mobile phone or laptop charging applications. As the power to be transferred increases, IPT becomes more attractive. Power transfer can be done in static [1] or dynamic mode [2]. Static charge is more preferred in terms of cost. In this study, static WPT was investigated. WPT, works like a loosely coupled transformer with a primary coil placed on the ground and a secondary coil fixed on the e-bike with an air-gap between these coils. Ferromagnetic cores improve the mutual coupling between the primary and secondary coil [3]. However, the use of cores affects the maximum destination of the vehicle as it increases the total weight. Generally WPT is made without any cores, considering the cost of the core selected for the high frequency and the core losses in the system operation.

Table 1. Frequencies and distances used in some designs

	Air-gap	**Frequency**
300W e-bike [3]	2 cm	40 kHz
560W city-car [4]	10 cm	85 kHz
1kW golf-cart [1]	15,6 cm	20,15 kHz
3,3 kW Sightseeing car [5]	15 cm	85,5 kHz
2 kW [6]	15 cm	19,8-20 kHz

Primary coil is supplied with a high frequency inverter for the wireless charging. Charge regulator part is constituted with uncontrolled full wave rectifier and buck converter. That is, a buck converter is added to the output of a typical resonance converter for charging in constant current / voltage mode. In order to keep the output voltage or current constant, the inverter input voltage or duty ratio can be controlled. However, a wireless communication system is required between the secondary and the primary.

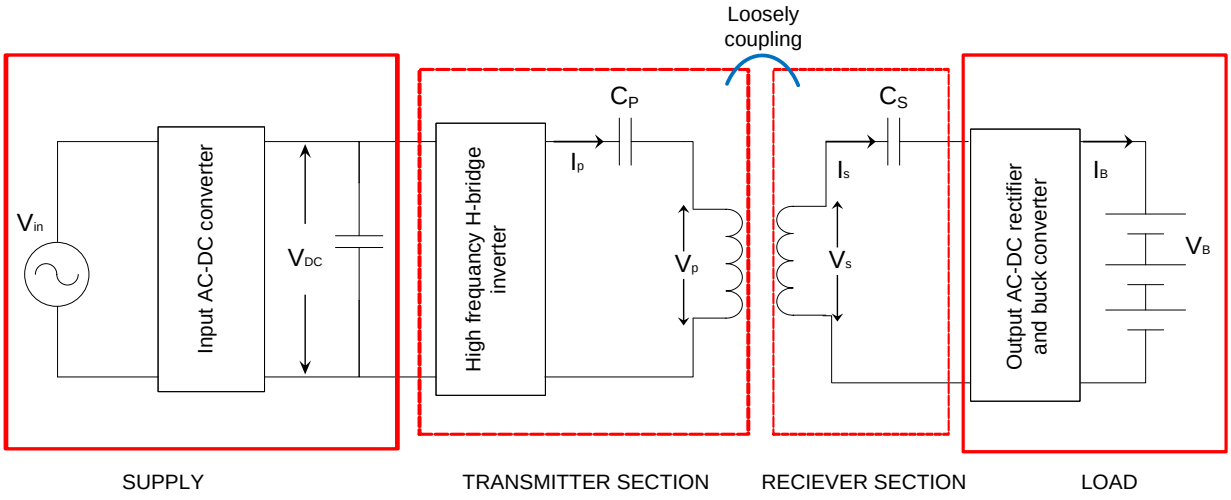

Figure 1. General Shame of the wireless charging

In this study, we preferred the use of buck converter for charge control on the secondary side without the need of communication. The general view of the WPT is given in Figure 1. In this study, firstly, general system constraints and design criteria are described, and then the overall WPT performance is investigated by explaining the used inverter and charge circuit.

2. General System Operation and Design Constraints

In a typical resonance converter, Series-Series (SS), Series-Parallel (SP), Parallel-Parallel (PP) and Parallel-Series (PS) compensation circuits can be used according to the characteristics of the source

and load. Generally, SS topology is used in static battery charging applications of EVs [10, 11]. The power transfer efficiency can be maximum if the receiver circuit operates at the resonance frequency. Similarly, the transmitter circuit should also operate in resonant mode for reactive power compensation. Thus, the values of the capacitors to be used in the primary (C_p) and the secondary (C_s) are determined as Eq. (1). Here L_p and L_s are self-inductance of the primer and seconder coil, respectively.

$$w_0 = \frac{1}{\sqrt{L_p C_p}} = \frac{1}{\sqrt{L_S C_S}} \tag{1}$$

Table 2. Design criteria of WPT

Parameter	Value
V_{dc}	30 V
V_B (max)	44V
I_B (max)	2,3 A
Distance	75 mm
Frequency	20.13 kHz

The general design criteria of the WPT considered in this study are given in Table 2. Firstly, it is necessary to determine what the secondary power and efficiency are depend on to improve in loosely coupling systems. Therefore, the electrical equivalent circuit of the primary and secondary should be examined (Figure 2).

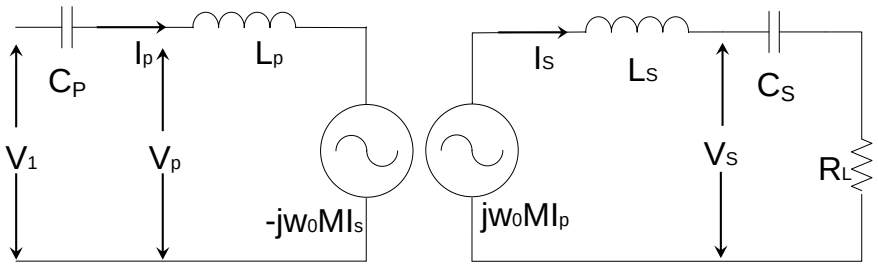

Figure 2. Equivalent circuit of compensated mutually

According to maximum power theory, the power in a compensated coil is calculated by Eq. (2). When the seconder circuit operates at the resonance frequency, the seconder current and voltage (I_S and V_S) equal to Eq. (3) and (4), respectively. Where, M is mutual inductance and R_L is equivalent load.

$$S_S = V_S x (I_S)^* \tag{2}$$

$$I_S = \frac{jw_0 M I_P}{R_L} \tag{3}$$

$$V_S = jw_0 M I_P \left[1 - \frac{jw_0 L_S}{R_L}\right] \tag{4}$$

Here, $\frac{w_0 L_S}{R_L}$ the secondary quality factor and is denoted by Q_S. In this case the secondary power;

$$S_S = \frac{w_0 (MI_P)^2}{L_S} Q_S (1 - jQ_S) \quad (5)$$

Assuming that the self and mutual inductance of the coils in the WPT system is constant in stationary charging, in the other words there is no any misalignment, the transmitted power depends on the operating frequency and primary current. Primary current is limited by the current density of the used conductor. Operating frequency can be selected between 5-140 kHz or higher in low power WPT systems [12]. Some WPT applications operate at high frequencies such as 80-100 kHz [4, 5], but in this study we have set the resonance frequency to 20 kHz, taking into account the switching losses and cost.

The output power and copper losses are considered to calculating the power transfer efficiency of the coils in a coreless WPT system as Eq. (6) and (7). Where R_p and R_S are the internal resistances of the primary and secondary windings, respectively.

$$\eta = \frac{R_L I_S^2}{R_P I_P^2 + R_S I_S^2 + R_L I_S^2} \quad (6)$$

$$\eta = \frac{R_L}{R_P \left(\frac{I_P}{I_S}\right)^2 + R_S + R_L} \quad (7)$$

If the current ratios in Eq. (3) are substituted in (7);

$$\eta = \frac{R_L}{R_S + R_L \left[1 + \frac{R_P (R_S + R_L)}{(wM)^2}\right]} \quad (8)$$

As seen in (8), if the resonance frequency increases, the power transfers efficiency of the coils increases too. Ordinarily, the power transfer circuit has one operating frequency. However, the secondary quality factor changes with the change of R_L load. In the same way, the coupling coefficient changes with the misalignment errors. Depending on these, there may be three operating resonance frequencies [13, 14]. This is called frequency bifurcation. To avoid frequency bifurcation, the primer and secondary quality factors should be selected as follows [14]:

$$Q_S < \sqrt{\frac{1 + \sqrt{1 - k^2}}{2k^2}} \quad (9)$$

$$Q_P > \frac{4Q_S^3}{4Q_S^2 - 1} \quad (10)$$

Where k is the coupling coefficient and;

$$k = \frac{M}{\sqrt{L_P L_S}} \quad (11)$$

3. Structure of Inverter

The charge control can be performed on the primary-side or secondary side in stationary WPT. Control variables on the primary side are DC source voltage, switching frequency and duty cycle. However, the current and voltage information of the load must be received by wireless communication for the control from the primary side. On the other hand, a DC-DC converter is used to control the secondary side. However, secondary-side control can be used in both static and dynamic systems.

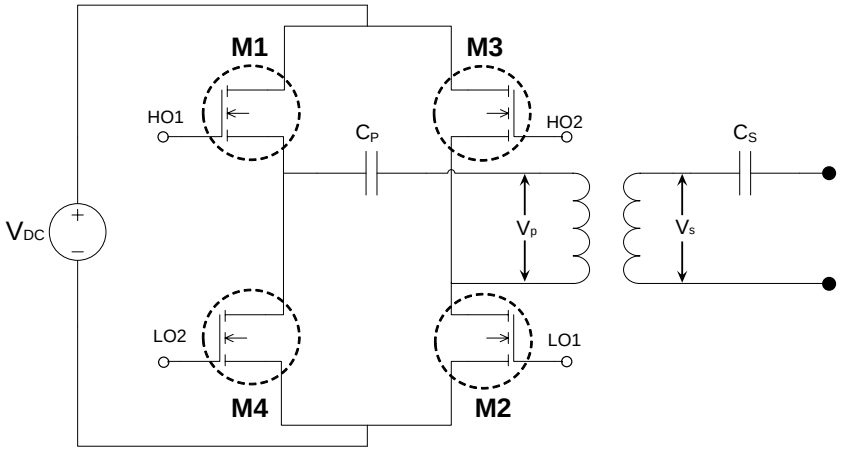

Figure 3. High frequency full-bridge inverter

In this study, a conventional full-bridge inverter is used at the fixed frequency as the control of the secondary-side is preferred (Figure 3). There are 17% dead time between two MOSFET (IRF2807) trigger signal to prevent short circuits. Figure 4 shows the switching signals of the MOSFETs. The DC voltage applied to the inverter input is set to 30V.

4. Coil Design

Litz wire is generally used to reduce the skin and proximity effects, due to operating frequency in the WPT design. The coil shape may be circular, square or rectangular. Alternatively, DD and DDQ structures are also proposed to reduce misalignment errors [15]. In this study, rectangular primary and secondary coil is used to make the best use of the area on the bicycle chassis. While the coil package is constituted, aluminum shielding can be used to reduce magnetic fringing in coreless design. However, the shielding and any part of core were not used to increase the weight in this study.

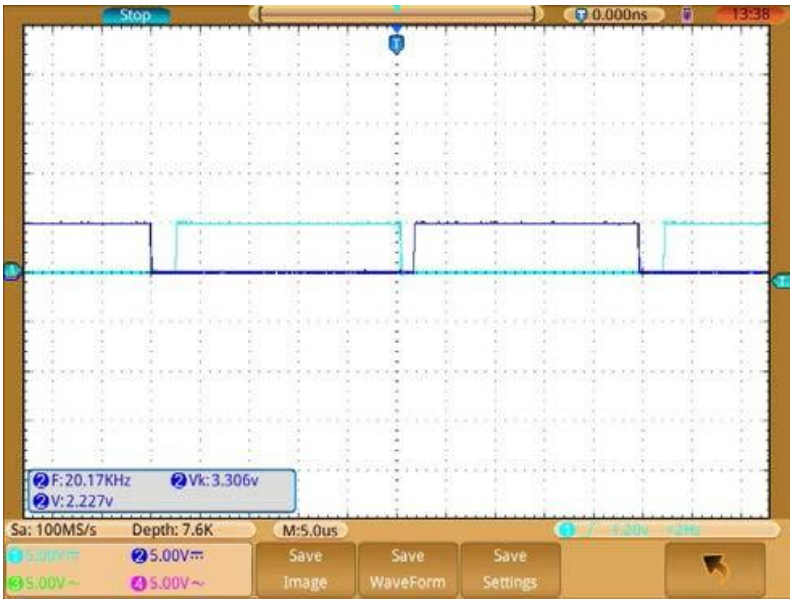

Figure 4. Gate signal of the M1 and M4

The winding dimensions and the number of turns are determined by taking into account the working criteria and constraints. Primer is produced as 213.88x253.88 mm outer dimensions and number of turns is 28, the secondary dimension is 225.98x265.98 mm and number of turns is equal to 38. The determined primary and secondary coils according to the design criteria were analyzed by the finite element method. Figure 5 shows the WPT model used in the FEA. The primary and secondary self-

inductances and mutual inductance were calculated as 244.26 and 398.6 and 82.95 µH, respectively in FEA. Primary and secondary self-inductances are measured as 270.3 and 430.7 µH in experimentally. Thus, the capacitors required for resonance, primary and secondary currents and voltages can be determined.

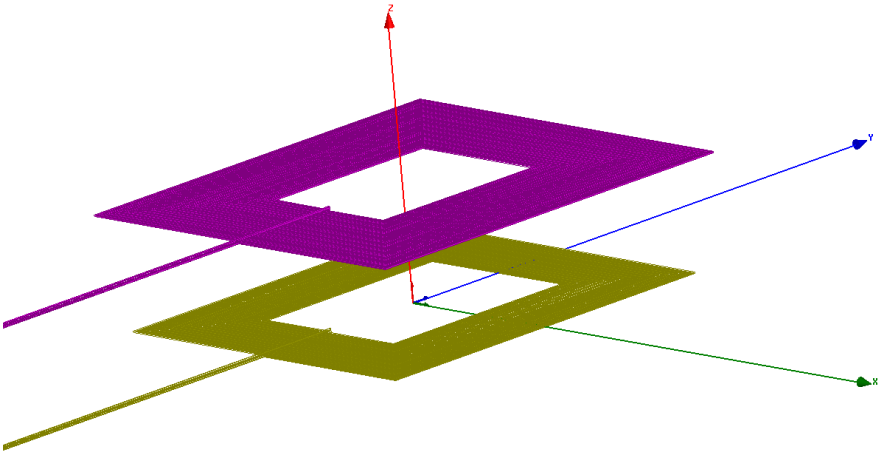

Figure 5. 3D FEA model of the WPT

5. Charging Circuit

The high frequency voltage in the secondary resonance circuit is first converted to DC with an uncontrolled rectifier by using fast diodes (DSEP15-06B) and then applied to the charge circuit. The charge of the lead acid battery is carried out at constant current (CC) or at constant voltage (CV) depending on the state of battery charge. If the voltage of the battery bank is below 44V, charging starts with CC mode. The constant charge current is determined as 2.3 A according to the battery datasheet. Data from the current and voltage sensors (values are 0.01 ohms) in the battery circuit are transmitted to the controller. When the voltage of the battery group reaches to 44V, charging continues with CV mode. The trigger signal of the MOSFET in the buck converter is controlled according to the received current and voltage information.

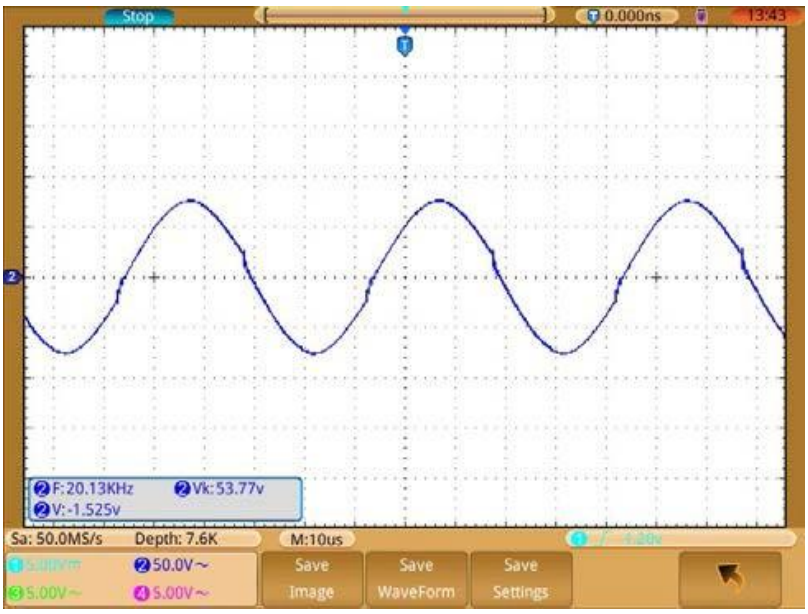

Figure 6. Wave form of the secondary voltage V_2

The waveform of the V_2 voltage transferred to the secondary at full load (44V and 2.3A) is shown in Figure 6. Small refractions are seen in the waveform of the V_2. If the operating frequency is far

away from the resonance frequency, these distortions will go up. The general diagram of the charge regulator is given in Figure 7. The L and C_{out} values in the buck converter topology are calculated as Eq. (12) and (13).

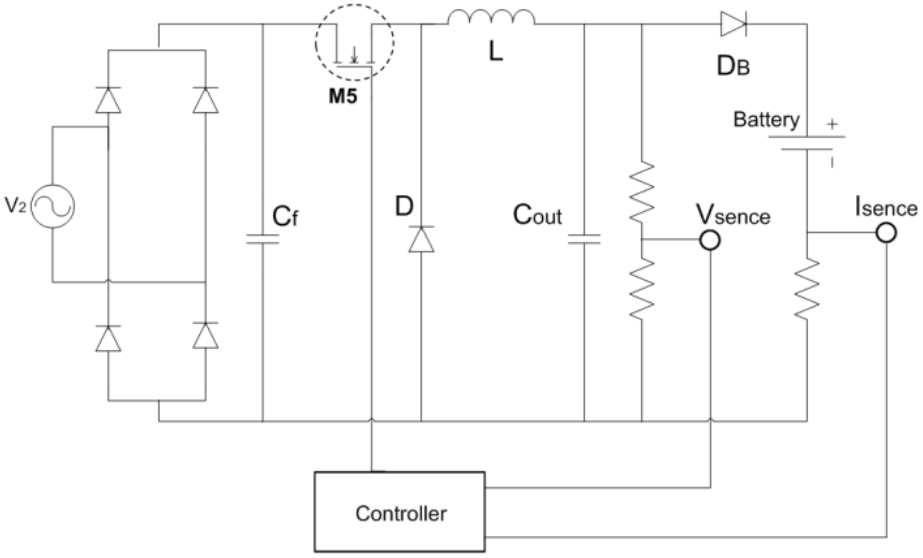

Figure 7. General shame of the charge regulator

Inductor ripple current and output capacitor ripple voltage has been selected as %1 to protect of lead acide battery. During this time, switching frequency has been set as 100 kHz because of to gain from PCB dimension.

$$\Delta I_L = \frac{(V_{IN} - V_{OUT})x\ D_{MAX}}{f_{sw}\ x\ L} \tag{12}$$

$$C_{OUT} = \frac{\Delta I_L}{8\ xf_{sw}\ x\ \Delta V_{OUT}} \tag{13}$$

Two feedback mechanisms are created for CC and CV mode that use. The current feedback has been kept constant with the aid of sense resistor and battery voltage feedback have been measured from terminals with voltage divider resistor. First of all, battery voltage is measured. According to feedback that comes, battery voltage is increased until to current value that want.

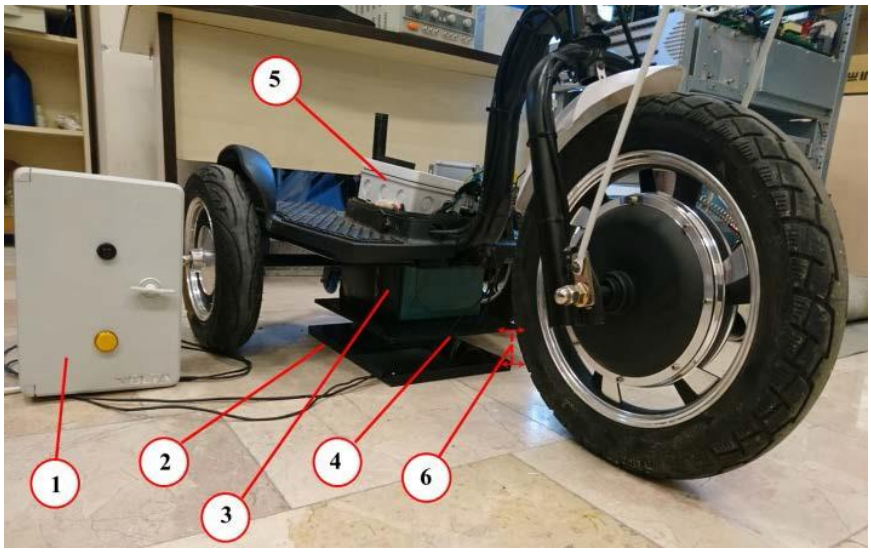

Figure 8. Experimental test setup: (1) inverter, (2) primary coil, (3) batteries, (4) secondary coil, (5) charge unit, (6) 75 mm distance

6. Experimental Results

The primary and secondary pads are positioned exactly concentric during the test (Figure 8). The distance between the primary and secondary pads is equal to 75 mm. The e-bike has three 12 V 20 Ah lead acid batteries connected in series. The experimental study was performed when the battery charge level was low. Figure 9 shows the measured current and voltage of the battery during charging in half-hourly periods.

The charge starts in CC mode since the voltage measured from the battery has been less than 44 V. This value is determined by looking at the datasheet of the battery. Charging continues in CC mode until the voltage of the battery group reaches 44 V. After the voltage is equal to 44 V, it goes into CV mode. In this way the current through the batteries starts to decrease. When the battery current drops to 0.3 A, the charge is finished, and the battery voltage is fixed to 41.5 V in stand-by mode.

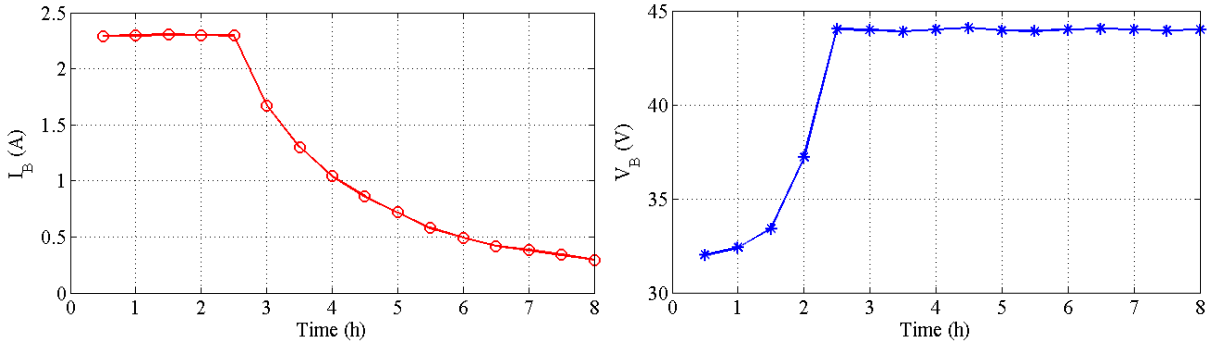

(a) (b)

Figure 9. The Current (a) and voltage (b) amplitude of the battery bank during charging

7. Conclusions

In this study, IPT system design has been made considering the physical constraints of the e-bike. The mutual and self-inductances of the primary and secondary windings determined according to the desired power and operating frequency have been calculated numerically in real 3D models. The measured inductances in the produced windings are close to the numerically calculated values. We can say that the system is almost at the resonant frequency by looking at the voltage waveform at the rectifier input. During charging, the power of the charging circuit as well as the inverter input power change. Experimental results were taken at different charge levels of the battery. The maximum total system efficiency (between the inverter supply and the charge circuit output) was 72% when operating in constant current mode. At this time, the transferred power is 101W and DC source is measured as 4.68A. The biggest power loss is on the rectifier diodes. The charging process is carried out safely in 8 hours in accordance with the characteristics of the battery. However, if desired, the controls for fast charging mode can be revised.

Acknowledgement

We would like to thank Volta Motor A.Ş. for their uninterrupted support during the study.

References

[1]. Kim, H., Song, C., Kim, D.Y., Jung, D.H., Kim, I.M., Kim, Y., Kim, J., Ahn, S., Kim, J., Coil Design and Measurements of Automotive Magnetic Resonant Wireless Charging System for High-Efficiency and Low Magnetic Field Leakage, in IEEE Transactions on Microwave Theory and Techniques, 2016, 64(2), 383-400.

[2]. Hao, H., Covic, G. A., Boys, J. T., An Approximate Dynamic Model of LCL-T-Based Inductive Power Transfer Power Supplies, in IEEE Transactions on Power Electronics, 2014, 29(10), 5554-5567.
[3]. Lanzuzi, D., Rubino, L., Noia, L.P.D., Rubino, G., Marino, P., Resonant Inductive Power Pransfer for An E-bike Charging Station, Electric Power Systems Research, 2016, 140, 631-642.
[4]. Buja, G., Bertoluzzo, M., Mude, K. N., Design and Experimentation of WPT Charger for Electric City Car, in IEEE Transactions on Industrial Electronics, 2015, 62(12), 7436-7447.
[5]. Li, Z., Zhu, C., Jiang, J., Song, K., Wei, G., A 3-kW Wireless Power Transfer System for Sightseeing Car Super capacitor Charge, in IEEE Transactions on Power Electronics, 2017, 32(5), 3301-3316.
[6]. Sallan, J., Villa, J. L., Llombart, A., Sanz, J. F., Optimal Design of ICPT Systems Applied to Electric Vehicle Battery Charge, in IEEE Transactions on Industrial Electronics, 56(6), 2009, 2140-2149.
[7]. Stielau, O. H., Covic, G. A., Design of Loosely Coupled Inductive Power Transfer Systems, International Conference on Power System Technology (PowerCon 2000). 4-7 Dec. 2000, Perth, WA, Australia, Australia, vol. 1, pp. 85-90.
[8]. Dieckerhoff, S., Ruan, M. J., De Doncker, R. W., Design of an IGBT-based LCL-resonant Inverter for High- Frequency Induction Heating," IEEE Industry Applications Conference. 3-7 Oct. 1999, Phoenix, AZ, USA, USA, vol. 3, pp. 2039-2045.
[9]. Keeling, N. A., Covic, G. A., Boys, J. T., A Unity- Power-Factor IPT Pickup for High-Power Applications, in IEEE Transactions on Industrial Electronics, 2010, 57(2), 744-751.
[10]. Huang, Z., Wong, S. C., Tse, C. K., Design Methodology of A Series-Series Inductive Power Transfer System for Electric Vehicle Battery Charger Application, IEEE Energy Conversion Congress and Exposition (ECCE), 14-18 Sept. 2014, Pittsburgh, PA, USA, pp. 1778-1782.
[11]. Mai, R., Chen, Y., Li, Y., Zhang, Y., Cao, G., He, Z., Inductive Power Transfer for Massive Electric Bicycles Charging Based on Hybrid Topology Switching With a Single Inverter, in IEEE Transactions on Power Electronics, 2017, 32(8), 5897-5906.
[12]. Covic, G. A., Boys, J. T., Inductive Power Transfer, in Proceedings of the IEEE, 2013, 101(6), 1276-1289.
[13]. Wang, C.S., Covic, G. A., Stielau, O. H., General Stability Criterions for Zero Phase Angle Controlled Loosely Coupled Inductive Power Transfer Systems, Industrial Electronics Society, (IECON '01). 29 Nov.-2 Dec. 2001, Denver, CO, USA, USA, vol. 2, pp. 1049-1054.
[14]. Aming, F., Haihong, Q., Zhixin, M., Pingyan, P., Analysis of Bifurcation Phenomena Based on Optimized Transformer in Loosely Coupled Inductive Power Transfer System, International Conference on Electrical and Control Engineering, 25-27 June 2010, Wuhan, China. pp. 3324-3327.
[15]. Budhia, M., Boys, J. T., Covic, G. A., Huang, C. Y., Development of a Single-Sided Flux Magnetic Coupler for Electric Vehicle IPT Charging Systems, in IEEE Transactions on Industrial Electronics, 2013, 60(1), 318-328.